Article

Fc-engineered antibody therapeutics with improved anti-SARS-CoV-2 efficacy

Check for updates

Rachel Yamin[1,5], Andrew T. Jones[1,5], Hans-Heinrich Hoffmann[2], Alexandra Schäfer[3], Kevin S. Kao[1], Rebecca L. Francis[1], Timothy P. Sheahan[3], Ralph S. Baric[3,4], Charles M. Rice[2], Jeffrey V. Ravetch[1,6 ✉] & Stylianos Bournazos[1,6 ✉]

Monoclonal antibodies with neutralizing activity against SARS-CoV-2 have demonstrated clinical benefits in cases of mild-to-moderate SARS-CoV-2 infection, substantially reducing the risk for hospitalization and severe disease[1–4]. Treatment generally requires the administration of high doses of these monoclonal antibodies and has limited efficacy in preventing disease complications or mortality among hospitalized patients with COVID-19[5]. Here we report the development and evaluation of anti-SARS-CoV-2 monoclonal antibodies with optimized Fc domains that show superior potency for prevention or treatment of COVID-19. Using several animal disease models of COVID-19[6,7], we demonstrate that selective engagement of activating Fcγ receptors results in improved efficacy in both preventing and treating disease-induced weight loss and mortality, significantly reducing the dose required to confer full protection against SARS-CoV-2 challenge and for treatment of pre-infected animals. Our results highlight the importance of Fcγ receptor pathways in driving antibody-mediated antiviral immunity and exclude the possibility of pathogenic or disease-enhancing effects of Fcγ receptor engagement of anti-SARS-CoV-2 antibodies upon infection. These findings have important implications for the development of Fc-engineered monoclonal antibodies with optimal Fc-effector function and improved clinical efficacy against COVID-19 disease.
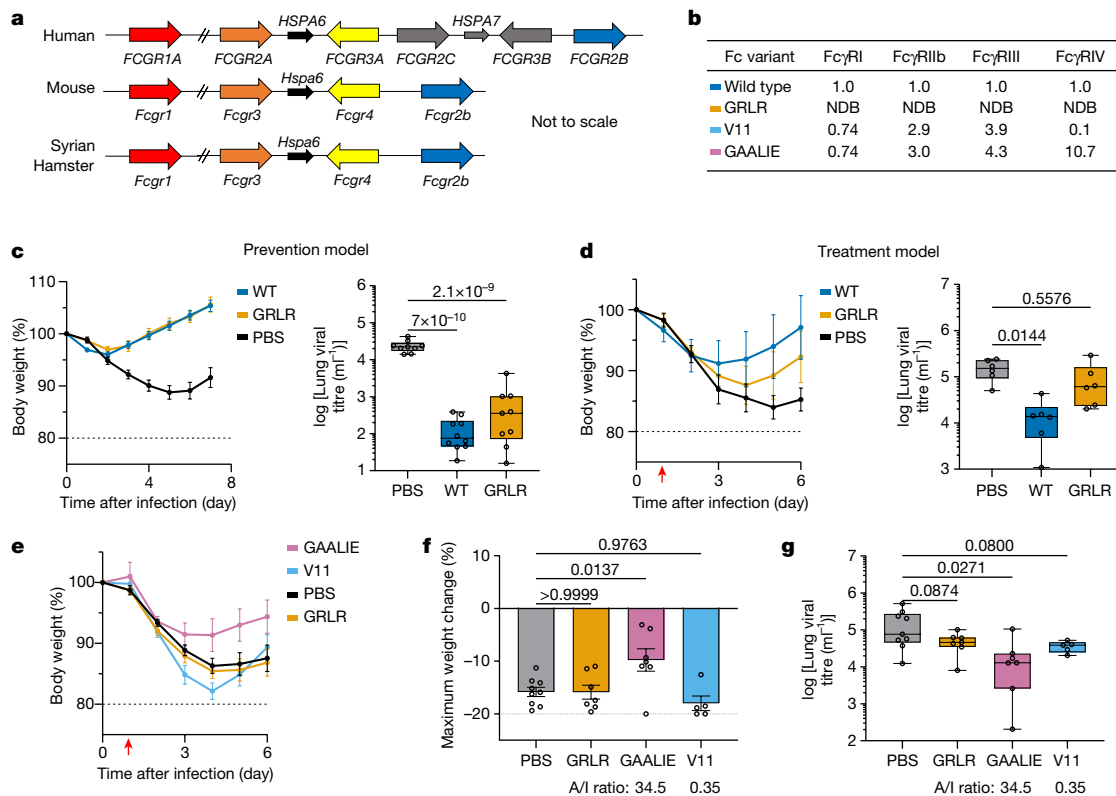
Several neutralizing monoclonal antibodies that target the SARS-CoV-2 spike protein have entered clinical testing over the past months, yielding US Food and Drug Administration approval of two monoclonal antibody cocktails—casirivimab and imdevimab, and bamlanivimab and etesevimab—for the treatment of patients with mild-to-moderate COVID-19[4]. In phase II/III studies, these and other monoclonal antibodies that are currently awaiting regulatory approval have demonstrated clear therapeutic benefits in cases of mild-to-moderate COVID-19, reducing the risk for hospitalization[1–3] by more than 80%. These results are in stark contrast to the findings from phase III trials (for example, ACTIV-3 and NCT04501978) that assessed the therapeutic activity of these monoclonal antibodies in hospitalized patients with COVID-19. In all cases, none of the tested monoclonal antibodies offered any therapeutic benefit, even when administered at exceedingly high doses or in combination with remdesivir[5].

The antiviral activity of IgG antibodies is the outcome of Fab-mediated virus neutralization coupled with the capacity of the Fc domain to mediate effector functions through interactions with Fcγ receptors (FcγRs) expressed on effector leukocytes[8]. FcγR engagement mediates pleiotropic functions, including the clearance of viral particles[9], cytotoxic elimination of virus-infected cells[10] and induction of antiviral T-cell responses[11]. Several reports, using well-defined in vivo models of SARS-CoV-2 infection, have independently demonstrated that the antiviral activity of neutralizing anti-SARS-CoV-2 antibodies depends on Fc–FcγR interactions[12–15]. In addition, mechanistic studies have shown that these protective effects are mediated primarily by CCR2^{+} monocytes, as well as cytotoxic CD8^{+} T cells that infiltrate the lung and confer antiviral activities[12]. Despite these findings, no studies have tested whether optimization of neutralizing anti-SARS-CoV-2 monoclonal antibodies for enhanced FcγR binding could improve their therapeutic activity, especially in the setting of severe COVID-19. Maximizing the capacity of neutralizing anti-SARS-CoV-2 monoclonal antibodies to engage and activate the appropriate FcγR pathways is expected to lower the monoclonal antibody dose required for the treatment of mild-to-moderate COVID-19, as well as improve their activity in hospitalized patients.

Currently, most monoclonal antibodies in clinical use or development are expressed as human IgG1, which—despite its affinity for activating FcγRs—also exhibits binding to the inhibitory FcγRIIb, thereby limiting protective Fc-effector activities[11]. In addition, owing to presumptive safety concerns over the capacity of antibodies to exacerbate disease through antibody-dependent enhancement (ADE) mechanisms[8], several clinical monoclonal antibodies (etesevimab, AZD8895 and AZD1061) have been engineered to lack FcγR-binding activity. However, despite numerous in vivo studies in animal models, there is no evidence for ADE[12–16], and therapeutic administration of high doses

[1]Laboratory of Molecular Genetics and Immunology, The Rockefeller University, New York, NY, USA. [2]Laboratory of Virology and Infectious Disease, The Rockefeller University, New York, NY, USA. [3]Department of Epidemiology, University of North Carolina at Chapel Hill, Chapel Hill, NC, USA. [4]Department of Microbiology and Immunology, University of North Carolina at Chapel Hill, Chapel Hill, NC, USA. [5]These authors contributed equally: Rachel Yamin and Andrew T. Jones. [6]These authors jointly supervised this work: Jeffrey V. Ravetch and Stylianos Bournazos. ✉e-mail: ravetch@rockefeller.edu; sbournazos@rockefeller.edu

Fig. 1 | Contribution of Fc-effector function to the protective activity of neutralizing anti-SARS-CoV-2 monoclonal antibodies in hamster infection models. a, Overview of the organization of FcγR gene loci in humans, mice and Syrian hamsters. **b**, Fc variants of human IgG1 were evaluated for their affinity for hamster FcγRs. Numbers indicate the fold change in affinity compared with wild-type human IgG1. NDB, no detectable binding. **c**, **d**, Wild-type (WT) and FcR-null (GRLR) variants of REGN monoclonal antibody cocktail (**c**) or S309 monoclonal antibody (**d**) were administered intravenously (5 mg kg^{−1}) to Syrian hamsters 1 day before (prevention model) (**c**) or 1 day after (therapy model) (**d**) intranasal challenge with SARS-CoV-2 (NYC isolate, 10[5] plaque-forming units (pfu)). $n = 9$ hamsters per group for PBS and GRLR-treated, $n = 10$ for wild-type from two independent experiments (**c**); $n = 6$ hamsters per group from two independent experiments (**d**). Hamsters were monitored for weight loss (left) (mean ± s.e.m.), and lung viral titres (right, analysed on day 7 (**c**) or day 6 (**d**) after infection) were compared between treatment groups by one-way ANOVA (Bonferroni post hoc analysis, adjusted for multiple comparisons). *P* values are indicated. **e**–**g**, SARS-CoV-2-infected hamsters (NYC isolate, 10[5] pfu) were treated on day 1 after infection with Fc variants of the REGN monoclonal antibody cocktail (5 mg kg^{−1}, intravenous injection) exhibiting differential hamster FcγR-binding affinity and activating-to-inhibitory (A/I) ratio (calculated on the basis of FcγRIV affinity/FcγRIIb affinity). Weight loss—plotted over time (mean ± s.e.m.) (**e**) or as maximum change (**f**)—and lung viral titres, assessed on day 6 after infection (**g**) were compared by one-way ANOVA (Bonferroni post hoc analysis adjusted for multiple comparisons). *P* values are indicated. $n = 9$ hamsters per group for PBS-treated, $n = 7$ for GRLR and GAALIE, and $n = 5$ for V11 from two independent experiments. Red arrow indicates time point of monoclonal antibody treatment post-infection. In box plots, the centre line shows the median, boxes represent the middle quartiles and whiskers show the range of values (minimum to maximum).
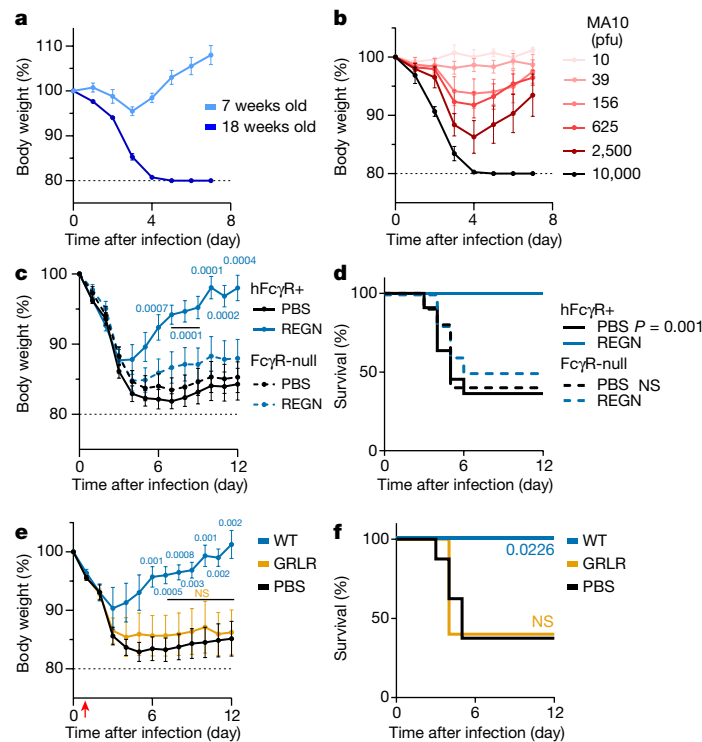
of convalescent plasma or neutralizing anti-SARS-CoV-2 monoclonal antibodies in patients with COVID-19 has not been associated with worse disease outcomes[1–3,5,17]. Similarly, comparable safety profiles were evident in clinical trials of neutralizing monoclonal antibodies with intact or diminished Fc-effector function[3,18,19].

Hamster FcγRs and IgG Fc-domain activity

To assess the role of FcγRs in the monoclonal antibody-mediated protection and develop monoclonal antibodies with superior therapeutic potency, we selected well-established small-animal models of SARS-CoV-2 infection that recapitulate the clinical features of human COVID-19[6,7,20]. One of these models involves the use of Syrian hamsters (*Mesocricetus auratus*), a species that sustains productive SARS-CoV-2 replication and exhibits evidence of severe disease upon challenge[6]. However, a major obstacle in the study of human IgG Fc-effector activity is the substantial interspecies differences in the affinity of human IgG antibodies for FcγRs expressed by rodent species such as hamsters[21]. We therefore cloned the four classes of hamster FcγRs and characterized their affinities for human, hamster and mouse IgG subclasses and Fc variants (Fig. 1a, b, Extended Data Fig. 1). Comparative analysis

of hamster FcγRs revealed substantial sequence homology to mouse FcγRs, with three hamster FcγRs (FcγRI, FcγRIII and FcγRIV) corresponding to activating FcγRs, whereas FcγRIIb represents the sole inhibitory FcγR.

To assess the contribution of Fc–FcγR interactions to monoclonal antibody-mediated protection, we selected neutralizing monoclonal antibodies that are in clinical use or development, including casirivimab and imdevimab (REGN cocktail[22]) and S309/VIR-7831[23] (Vir) and expressed them as human IgG1 or as Fc variants with defined affinity for hamster FcγRs. In agreement with recent reports[12], we observed that when monoclonal antibodies are administered prophylactically, Fc-effector function shows minimal contribution to their antiviral activity (Fig. 1c). By contrast, in the therapeutic setting, wild-type, but not FcR-null (GRLR) variants, are able to suppress lung viremia and prevent weight loss (Fig. 1d). Because previous studies in mouse models of influenza and HIV-1 infection support a key role for FcγRIV in monoclonal antibody-mediated protection[10,24], we compared the in vivo therapeutic activities of two Fc-domain variants—GAALIE and V11—that exhibit differential hamster FcγRIV-binding activity, but comparable affinity for the other hamster FcγRs (Fig. 1b). Whereas the FcγRIV-enhanced variant (GAALIE) demonstrates potent antiviral activity, no therapeutic

Fig. 2 | Fc–FcγR interactions are required for the therapeutic activity of neutralizing anti-SARS-CoV-2 monoclonal antibodies in mouse infection models. a, **b**, FcγR-humanized mice were infected with mouse-adapted SARS-CoV-2 (MA10 strain, 10^4 pfu, intranasal) and weight loss (mean ± s.e.m.) was compared in young (7 weeks old; $n = 5$) and older (18 weeks old; $n = 4$) mice (**a**), as well as in mice (16 to 19 weeks old) challenged with the indicated inoculum dose (**b**). $n = 5$ mice per group; $n = 4$ for 10^4 and 10 pfu dose groups from two independent experiments. **c**, **d**, The therapeutic activity of REGN monoclonal antibody cocktail (expressed as human IgG1 and administered at 5 mg kg^{-1} 1 day after infection) was evaluated in FcγR-humanized (hFcγR+) and FcγR-deficient (FcγR-null) mouse strains challenged with SARS-CoV-2 (MA10 strain, 10^4 pfu, intranasal). $n = 10$ mice per group (FcγR-null); $n = 11$ (PBS) and $n = 12$ (REGN) mice per group for FcγR-humanized mice from two independent experiments. **e**, **f**, SARS-CoV-2-infected FcγR-humanized mice (MA10 strain, 10^4 pfu, intranasal) were treated with wild-type human IgG1 or GRLR variants of REGN monoclonal antibody cocktail 1 day after infection. $n = 8$ (PBS), $n = 5$ (wild-type) and $n = 6$ (GRLR) mice per group from two independent experiments. Weight loss (**c**, **e**; mean ± s.e.m.) and survival curves (**d**, **f**) were compared to the corresponding PBS-treated group by two-way ANOVA (Bonferroni post hoc analysis adjusted for multiple comparisons) and log-rank (Mantel–Cox) test, respectively. P values are indicated. NS, not significant. Red arrow indicates time point of monoclonal antibody treatment post-infection.

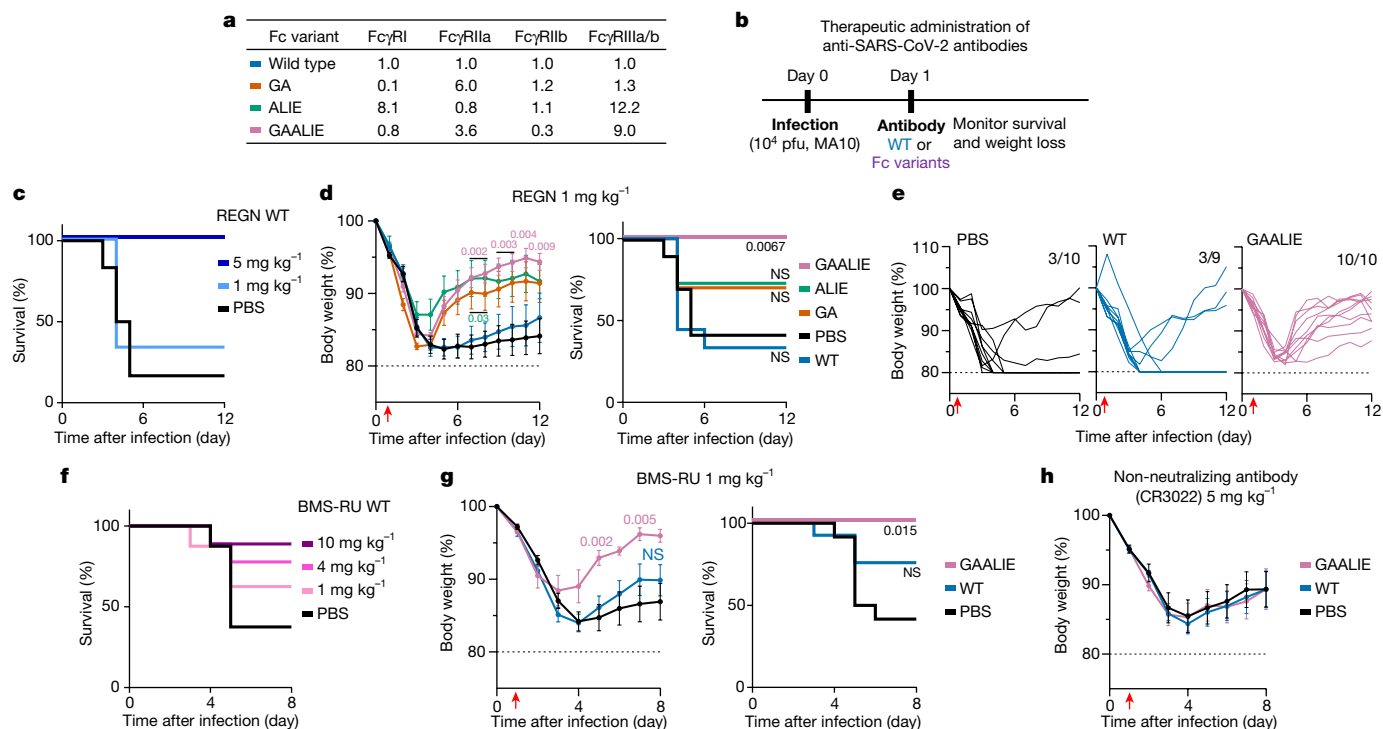activity is evident for V11, which exhibits minimal affinity for hamster FcγRIV (Fig. 1e–g).

SARS-CoV-2 in FcγR-humanized mice

Although these findings support the importance of Fc–FcγR interactions in monoclonal antibody-mediated protection against SARS-CoV-2 infection, their translational relevance is limited, given the structural complexity of the FcγR family and the divergence of these receptors between humans and other mammalian species[21]. To address this problem, we previously developed a mouse strain in which only human FcγRs are expressed in a pattern that recapitulates as faithfully as possible the expression pattern in human tissues[25]. Despite differences in the absolute FcγR expression levels between humans and FcγR-humanized mice (for example, the expression of FcγRI on neutrophils and FcγRIIb on monocytes), this strain represents a suitable platform for studies on human IgG antibody function with translational relevance to humans. Human FcγR expression among the various leukocyte populations is stable and does not differ between young and old mice (Extended Data Fig. 2). Infection of old (more than 15-week-old), but not young (7-week-old), FcγR-humanized mice with the mouse-adapted SARS-CoV-2 strain MA10[7] results in challenge-dose-dependent weight loss and mortality (Fig. 2a, b). Recent studies have determined that on day 2 after infection, MA10-infected mice exhibit peak lung viral titres, accompanied by severely compromised pulmonary function and extensive lung histopathologic damage[7]. Histological evaluation of

lungs from MA10-infected FcγR-humanized mice (more than 15 weeks old) revealed multifocal areas of interstitial pneumonia, extensive inflammatory cell infiltration and occasional necrotic and proteinaceous material and hyalinized membranes within affected alveoli (Extended Data Fig. 3). Such histopathological findings are consistent with those observed in well-established animal models of SARS-CoV-2 infection used extensively in previous studies, and resemble the lung pathology of human COVID-19[7,12–14]. Although it is not classified as a variant of concern, the MA10 strain contains several mutations near the epitopes targeted by monoclonal antibodies currently in clinical use or development. As a result, several of these monoclonal antibodies exhibit significantly reduced neutralizing activity against MA10, which is comparable to that observed for variants of concern such as B1.351 (Extended Data Fig. 4).

Fc-effector function in antibody therapy

In a model of monoclonal antibody-mediated therapy, we observed that the REGN monoclonal antibody cocktail (expressed as wild-type human IgG1) confers full protection of FcγR-humanized mice when administered at 5 mg kg^{-1} 1 day after lethal challenge with MA10 (Fig. 2c–f). By contrast, no therapeutic activity is evident in mice lacking FcγRs (FcγR-null) or when monoclonal antibodies are expressed as variants (GRLR) with minimal affinity for human FcγRs, highlighting the importance of Fc-effector function in the therapeutic activity of neutralizing monoclonal antibodies (Fig. 2c–f). To determine the mechanisms by

Fig. 3 | Selective engagement of activating FcγRs improves the therapeutic activity of anti-SARS-CoV-2 monoclonal antibodies. a, Human IgG1 Fc variants with differential affinity for specific classes of human FcγRs were generated for anti-SARS-CoV-2 monoclonal antibodies. Numbers indicate the fold change in affinity compared with wild-type human IgG1. **b–g**, Following the experimental strategy shown in **b**, SARS-CoV-2-infected FcγR-humanized mice were treated intravenously at the indicated dose with REGN (**c–e**) or BMS-RU (**f, g**) monoclonal antibody cocktail, or the non-neutralizing monoclonal antibody CR3022 (**h**), expressed as wild-type human IgG1 (blue in **c–h**) or as Fc variants with differential affinity for human FcγRs (magenta in **c–h**). Weight loss (**d**, left, **g**, left, **h**; mean ± s.e.m.) (**e**; curves for individual mice) and survival curves (**c, d**, right, **f, g**, right) for antibody-treated mice were

compared with the corresponding PBS-treated group by two-way ANOVA (Bonferroni post hoc analysis adjusted for multiple comparisons) and log-rank (Mantel–Cox) test, respectively. The fraction of surviving mice is indicated in **e**. P values are indicated. **c**, $n = 6$ mice per group from two independent experiments; **d, e**, $n = 10$ mice per group (PBS, GAALIE and GA groups), $n = 9$ (wild-type) and $n = 11$ (ALIE) mice from four independent experiments; **f**, $n = 8$ (PBS and 1 mg kg^{-1}) or 9 (10 mg kg^{-1} and 4 mg kg^{-1}) mice per group from two independent experiments; **g**, $n = 7$ (GAALIE) or 12 (PBS and wild-type) mice per group from three independent experiments. **h**, $n = 8$ (GAALIE) or 10 (PBS and wild-type) mice per group from two independent experiments. Red arrow indicates time point of monoclonal antibody treatment post-infection.

which human FcγRs contribute to the monoclonal antibody-mediated protection, REGN cocktail monoclonal antibodies were expressed as human IgG1 Fc variants[11], and exhibit differential affinities for the various human FcγRs (Fig. 3a). As outlined in Fig. 3b, we assessed the therapeutic activity of Fc variants of the REGN monoclonal antibody cocktail at a dose (1 mg kg^{-1}) at which wild-type human IgG1 confers minimal protection (Fig. 3c). Consistent with a protective role for activating FcγRs, Fc variants enhanced for either FcγRIIa (GA) or FcγRI and FcγRIII (ALIE) show a trend of improved therapeutic potency over wild-type IgG1, whereas maximal therapeutic activity was evident only for the GAALIE variant, which is enhanced for both FcγRIIa and FcγRIII and has reduced affinity for the inhibitory FcγRIIb (Fig. 3d, e). These findings suggest that synergy between the two activating FcγRs—FcγRIIa and FcγRIII—probably accounts for the therapeutic activity of the GAALIE variant, which achieves the same degree of protection as wild-type IgG1, but at a fivefold lower dose. Additionally, the observed differences in the in vivo therapeutic activity among Fc variants could not be attributed to differences in their in vitro neutralization activity, antigen binding specificity or in vivo half-life (Extended Data Figs. 5, 6).
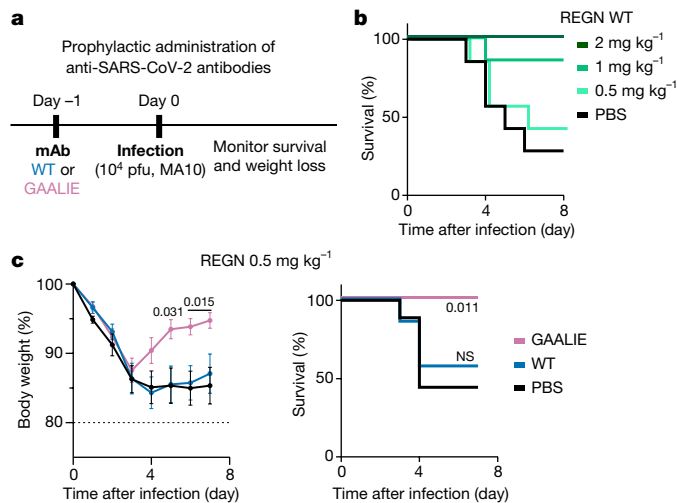
Notably, treatment of MA10-infected mice 1 day after infection with the GAALIE variant was not associated with enhanced disease, when administered at a low dose (1 mg kg^{-1}) or at a much higher dose (40 mg kg^{-1}) (Extended Data Fig. 7a). At this higher dose, which is typically used in the clinical setting, FcR-null variants (GRLR) also exhibit full protective activity similar to the GAALIE variants, suggesting that Fc-independent protection could be achieved once neutralizing

monoclonal antibodies are administered at sufficiently high doses, as has been documented previously for other viral pathogens[24]. Similarly, treatment of SARS-CoV-2-infected mice two days after infection, which coincides with the peak of lung viral replication[7], has no disease-enhancing effects and neither GAALIE nor GRLR variants offer any therapeutic benefit, confirming recent reports showing that the therapeutic window for neutralizing monoclonal antibodies is limited to 24 h after infection[26] (Extended Data Fig. 7b).

Similar results were obtained when we assessed the in vivo therapeutic activity of another neutralizing anti-SARS-CoV-2 monoclonal antibody cocktail[27] (C135 + C144 (also known as BMS-RU)) currently in clinical development[27]. When BMS-RU is administered to FcγR-humanized mice at 1 mg kg^{-1}, only GAALIE variants, but not wild-type human IgG1 confer protective activity and prevent disease-induced weight loss (Fig. 3f, g). In contrast to neutralizing anti-SARS-CoV-2 monoclonal antibodies, Fc-engineering of the non-neutralizing anti-receptor-binding domain (RBD) monoclonal antibody CR3022 does not result in improved therapeutic activity, as neither CR3022-GAALIE nor CR3022 protected mice from lethal SARS-CoV-2 challenge (Fig. 3h).

Fc-domain activity in antibody prophylaxis

Our findings in hamsters suggest that when neutralizing monoclonal antibodies are administered prophylactically, Fc–FcγR interactions are not critical for their antiviral activity (Fig. 1c). However, given the substantial interspecies differences in FcγR biology between hamsters and

Fig. 4 | Prophylactic activity of anti-SARS-CoV-2 monoclonal antibodies is enhanced by selective engagement of activating FcγRs. a–c, The activity of wild-type and GAALIE variants of the REGN monoclonal antibody cocktail was assessed in a model of monoclonal antibody (mAb)-mediated prophylaxis of SARS-CoV-2 infection (**a**). FcγR-humanized mice were treated (intravenously) at the indicated dose with REGN monoclonal antibody cocktail expressed as wild-type human IgG1 or as GAALIE variant one day before challenge with SARS-CoV-2 (MA10, 10^4 pfu, intranasal). Weight loss (mean ± s.e.m.) (**c**, left) and survival curves (**b**, **c**, right) of antibody-treated mice were compared with the PBS-treated group by two-way ANOVA (Bonferroni post hoc analysis adjusted for multiple comparisons) and log-rank (Mantel–Cox) test, respectively. P values are indicated. **b**, $n = 7$ mice per group ($n = 6$ mice per group for 2 mg kg^{-1}) from two independent experiments; **c**, $n = 7$ (wild-type) or 9 (PBS and GAALIE) mice per group from three independent experiments.

humans, we assessed the contribution of activating FcγR engagement to the monoclonal antibody-mediated prophylaxis of MA10-challenged FcγR-humanized mice (Fig. 4a). When administered at a dose at which wild-type human IgG1 exhibits no protective activity (0.5 mg kg^{-1}) (Fig. 4b), GAALIE variants of the REGN monoclonal antibody confer full protection against lethal SARS-CoV-2 challenge, suggesting that selective activating FcγR engagement could improve the efficacy of neutralizing monoclonal antibodies in both the therapeutic as well as in the prophylactic setting (Fig. 4c).

Discussion

To maximize the translational relevance of our findings, this study focused on neutralizing anti-SARS-CoV-2 monoclonal antibodies that are currently in clinical use or development and assessed their in vivo protective activity in mouse strains that recapitulate the unique complexity of human FcγRs[25]. Challenge of FcγR-humanized mice with MA10 results in accelerated weight loss and significant mortality, resembling the clinical manifestations of severe COVID-19. However, such rapid symptomatic disease development limits the therapeutic window for monoclonal antibody treatment and does not allow full unravelling of the mechanisms of COVID-19 disease pathogenesis and the potential immunopathologies due to host immune-related responses. Despite this limitation, we observed that in models of monoclonal antibody-mediated prophylaxis or early treatment, Fc engineering for selective binding to activating FcγRs resulted in an approximately fivefold reduction in the monoclonal antibody dose required to achieve full therapeutic benefit; a finding consistent with our recent in vivo evaluation studies on Fc-optimized anti-influenza virus monoclonal antibodies[11]. Consistent with previous studies on other viral pathogens, including HIV-1[28], influenza[24] and Ebola[29], our findings suggest that FcγR—but not complement pathways—confer monoclonal

antibody-mediated protection, as monoclonal antibodies lack protective activity in mice deficient for all classes of FcγRs (Fig. 2c, d). Moreover, Fc variants such as GAALIE, which exhibit diminished C1q-binding activity (Extended Data Fig. 8), demonstrate improved therapeutic efficacy compared with wild-type IgG1.

Analysis of IgG Fc glycan characteristics in hospitalized patients with COVID-19 has previously revealed an association of disease severity with increased levels of afucosylated glycoforms[30,31], which exhibit increased affinity for the activating FcγRIII[11]. Although these results suggest a potential pathogenic effect for FcγRIII pathways, patients with severe COVID-19 are also characterized by delayed induction of neutralizing antibody responses accompanied by elevated antibody levels[32], suggesting that any disease-enhancing effects of afucosylated antibodies might also be related to their poor neutralizing activity[33]. However, in our study, we did not observe any pathogenic or disease-enhancing effects of anti-SARS-CoV-2 monoclonal antibodies engineered for enhanced binding to activating FcγRs, irrespective of their neutralizing potency (Fig. 3). It is therefore probable that susceptibility to severe disease is not entirely driven by the FcγRIII-binding activity of anti-SARS-CoV-2 IgGs, but rather by multiple, complex immunological determinants.

Despite the successful deployment of highly effective vaccines, neutralizing anti-SARS-CoV-2 monoclonal antibodies are expected to continue to have an important role in virus-containment efforts and the clinical management of COVID-19, especially in high-risk populations and immunocompromised individuals. Although regulatory approval of anti-SARS-CoV-2 monoclonal antibody cocktails has been based on their remarkable clinical efficacy in patients with mild-to-moderate COVID-19[1–3], none of the currently approved monoclonal antibodies take full advantage of the potential of IgG molecules to mediate protective antiviral Fc-effector functions. Our findings provide a paradigm for the development of monoclonal antibody-based therapeutics with improved potency and superior therapeutic efficacy against COVID-19 through selective engagement of specific FcγR pathways.

Online content

Any methods, additional references, Nature Research reporting summaries, source data, extended data, supplementary information, acknowledgements, peer review information; details of author contributions and competing interests; and statements of data and code availability are available at https://doi.org/10.1038/s41586-021-04017-w.

1. Chen, P. et al. SARS-CoV-2 neutralizing antibody LY-CoV555 in outpatients with Covid-19. *N. Engl. J. Med.* **384**, 229–237 (2021).
2. Weinreich, D. M. et al. REGN-COV2, a neutralizing antibody cocktail, in outpatients with Covid-19. *N. Engl. J. Med.* **384**, 238–251 (2021).
3. Gottlieb, R. L. et al. Effect of bamlanivimab as monotherapy or in combination with etesevimab on viral load in patients with mild to moderate COVID-19: a randomized clinical trial. *JAMA* **325**, 632–644 (2021).
4. Taylor, P. C. et al. Neutralizing monoclonal antibodies for treatment of COVID-19. *Nat. Rev. Immunol.* **21**, 382–393 (2021).
5. Lundgren, J. D. et al. A neutralizing monoclonal antibody for hospitalized patients with Covid-19. *N. Engl. J. Med.* **384**, 905–914 (2021).
6. Sia, S. F. et al. Pathogenesis and transmission of SARS-CoV-2 in golden hamsters. *Nature* **583**, 834–838 (2020).
7. Leist, S. R. et al. A mouse-adapted SARS-CoV-2 induces acute lung injury and mortality in standard laboratory mice. *Cell* **183**, 1070–1085.e1012 (2020).
8. Bournazos, S., Gupta, A. & Ravetch, J. V. The role of IgG Fc receptors in antibody-dependent enhancement. *Nat. Rev. Immunol.* **20**, 633-643 (2020).
9. Bournazos, S. et al. Broadly neutralizing anti-HIV-1 antibodies require Fc effector functions for in vivo activity. *Cell* **158**, 1243–1253 (2014).
10. Lu, C. L. et al. Enhanced clearance of HIV-1-infected cells by broadly neutralizing antibodies against HIV-1 in vivo. *Science* **352**, 1001–1004 (2016).
11. Bournazos, S., Corti, D., Virgin, H. W. & Ravetch, J. V. Fc-optimized antibodies elicit CD8 immunity to viral respiratory infection. *Nature* **588**, 485–490 (2020).
12. Winkler, E. S. et al. Human neutralizing antibodies against SARS-CoV-2 require intact Fc effector functions for optimal therapeutic protection. *Cell* **184**, 1804–1820.e1816 (2021).
13. Suryadevara, N. et al. Neutralizing and protective human monoclonal antibodies recognizing the N-terminal domain of the SARS-CoV-2 spike protein. *Cell* **184**, 2316–2331.e2315 (2021).

Article

14. Schäfer, A. et al. Antibody potency, effector function, and combinations in protection and therapy for SARS-CoV-2 infection in vivo. *J. Exp. Med.* **218**, e20201993 (2021).
15. Ullah, I. et al. Live imaging of SARS-CoV-2 infection in mice reveals neutralizing antibodies require Fc function for optimal efficacy. Preprint at https://doi.org/10.1101/2021.03.22.436337 (2021).
16. Li, D. et al. The functions of SARS-CoV-2 neutralizing and infection-enhancing antibodies in vitro and in mice and nonhuman primates. Preprint at https://doi.org/10.1101/2020.12.31.424729 (2021).
17. Joyner, M. et al. Early safety indicators of COVID-19 convalescent plasma in 5,000 patients. *J. Clin. Invest.* **130**, 4791–4797 (2020).
18. Dougan, M. et al. Bamlanivimab plus etesevimab in mild or moderate Covid-19. *N. Engl. J. Med.* **385**, 1382–1392 (2021).
19. Wu, X. et al. Tolerability, safety, pharmacokinetics, and immunogenicity of a novel SARS-CoV-2 neutralizing antibody, etesevimab, in Chinese healthy adults: a randomized, double-blind, placebo-controlled, first-in-human phase 1 study. *Antimicrob. Agents Chemother.* **65**, e0035021 (2021).
20. Cleary, S. J. et al. Animal models of mechanisms of SARS-CoV-2 infection and COVID-19 pathology. *Br. J. Pharmacol.* **177**, 4851–4865 (2020).
21. Bournazos, S. IgG Fc receptors: evolutionary considerations. *Curr. Top. Microbiol. Immunol.* **423**, 1–11 (2019).
22. Baum, A. et al. REGN-COV2 antibodies prevent and treat SARS-CoV-2 infection in rhesus macaques and hamsters. *Science* **370**, 1110–1115 (2020).
23. Pinto, D. et al. Cross-neutralization of SARS-CoV-2 by a human monoclonal SARS-CoV antibody. *Nature* **583**, 290–295 (2020).
24. DiLillo, D. J., Tan, G. S., Palese, P. & Ravetch, J. V. Broadly neutralizing hemagglutinin stalk-specific antibodies require FcγR interactions for protection against influenza virus in vivo. *Nat. Med.* **20**, 143–151 (2014).
25. Smith, P., DiLillo, D. J., Bournazos, S., Li, F. & Ravetch, J. V. Mouse model recapitulating human Fcγ receptor structural and functional diversity. *Proc. Natl Acad. Sci. USA* **109**, 6181–6186 (2012).
26. Martinez, D. R. et al. Prevention and therapy of SARS-CoV-2 and the B.1.351 variant in mice. *Cell Rep.* **36**, 109450 (2021).
27. Wang, Z. et al. mRNA vaccine-elicited antibodies to SARS-CoV-2 and circulating variants. *Nature* **592**, 616–622 (2021).
28. Hessell, A. J. et al. Fc receptor but not complement binding is important in antibody protection against HIV. *Nature* **449**, 101–104 (2007).
29. Bournazos, S., DiLillo, D. J., Goff, A. J., Glass, P. J. & Ravetch, J. V. Differential requirements for FcγR engagement by protective antibodies against Ebola virus. *Proc. Natl Acad. Sci. USA* **116**, 20054–20062 (2019).
30. Chakraborty, S. et al. Proinflammatory IgG Fc structures in patients with severe COVID-19. *Nat. Immunol.* **22**, 67–73 (2021).
31. Larsen, M. D. et al. Afucosylated IgG characterizes enveloped viral responses and correlates with COVID-19 severity. *Science* **371**, eabc8378 (2021).
32. Lucas, C. et al. Delayed production of neutralizing antibodies correlates with fatal COVID-19. *Nat. Med.* **27**, 1178–1186 (2021).
33. Atyeo, C. et al. Dissecting strategies to tune the therapeutic potential of SARS-CoV-2-specific monoclonal antibody CR3022. *JCI Insight* **6**, e143129 (2021).

Methods

Viruses, cell lines and animals
A P1 stock of the SARS-CoV-2 MA10 strain[7] was amplified in VeroE6 cells obtained from the ATCC that were engineered to stably express TMPRSS2 (VeroE6-TMPRSS2). To generate a P2 working stock, VeroE6-TMPRSS2 cells were infected at a multiplicity of infection (MOI) of 0.1 pfu per cell and incubated at 37 °C for 4 days. The virus-containing supernatant was subsequently harvested, clarified by centrifugation ($3,000g$; 10 min), and filtered using a disposable vacuum filter system with a 0.22-μm membrane. Virus stock titres were measured by standard plaque assay on Huh-7.5 cells that stably express ACE2 and TMPRSS (Huh-7.5-ACE2/TMPRSS2). In brief, 500 μl of serial tenfold virus dilutions in Opti-MEM were used to infect 4×10^5 cells seeded the previous day into wells of a 6-well plate. After 90 min adsorption, the virus inoculum was removed, and cells were overlaid with DMEM containing 10% FBS with 1.2% microcrystalline cellulose (Avicel). Cells were incubated for 4 days at 33 °C, followed by fixation with 7% formaldehyde and crystal violet staining for plaque counting. To confirm virus identity and evaluate for unwanted mutations that were acquired during the amplification process, RNA from virus stocks was purified using TRIzol reagent (ThermoFisher). In brief, 200 μl of each virus stock was added to 800 μl TRIzol reagent, followed by 200 μl chloroform, which was then centrifuged at $12,000g$ for 5 min. The upper aqueous phase was moved to a new tube, mixed with an equal volume of isopropanol, and then added to an RNeasy Mini Kit column (Qiagen) to be further purified following the manufacturer's instructions. Viral stocks were subsequently confirmed by Next Generation Sequencing using libraries for Illumina MiSeq.

The SARS-CoV-2 NYC isolate was obtained from a patient's saliva generously provided by A. Viale (Memorial Sloan Kettering Cancer Center) and amplified in Caco-2 cells. This P1 virus was used to generate a P2 working stock by infecting Caco-2 cells at an MOI of 0.05 pfu per cell. Cells were incubated at 37 °C for 6 days before collecting virus-containing supernatant as described above. Similarly, virus stock titres were determined by plaque assay performed on Huh-7.5-ACE2/TMPRSS2 cells. All SARS-CoV-2 experiments were carried out in biosafety level 3 (BSL-3) containment in compliance with institutional and federal guidelines.

VeroE6 cells (ATCC, CRL-1586), Caco-2 cells (ATCC, HTB-37) and Huh-7.5 hepatoma cells[34] were cultured in Dulbecco's Modified Eagle Medium (DMEM) supplemented with 1% nonessential amino acids and 10% fetal bovine serum (FBS). The 293T cells (ATCC, CRL-3216) and HT1080-ACE2 (provided by P. Bieniasz (Rockefeller University)) were maintained in DMEM supplemented with 10% FBS, 50 U ml^{-1} penicillin and 50 μg ml^{-1} streptomycin (ThermoFisher). All cell lines were maintained at 37 °C at 5% CO_2. Expi293F cells (ThermoFisher) were maintained at 37 °C, 8% CO_2 in Expi293 expression medium (ThermoFisher) supplemented with 10 U ml^{-1} penicillin and 10 μg ml^{-1} streptomycin. Cell lines were not authenticated after purchase. All cell lines tested negative for mycoplasma contamination.

In vivo experiments were approved by the Rockefeller University Institutional Animal Care and Use Committee in compliance with federal laws and institutional guidelines. Hamsters and mice were maintained at the Comparative Bioscience Center at the Rockefeller University at a controlled ambient temperature (20–25 °C) and humidity (30–70%) environment with 12-h dark:light cycle. Golden Syrian hamsters were purchased from Charles River laboratories (strain code 049) and maintained in compliance with USDA regulations. FcγR knockout (mFcγRα$^{-/-}$; $Fcgr1^{-/-}$) and FcγR-humanized mice (mFcγRα$^{-/-}$, $Fcgr1^{-/-}$, hFcγRI$^+$, hFcγRIIa$_{R131}^+$, hFcγRIIb$^+$, hFcγRIIIa$_{F158}^+$ and hFcγRIIIb$^+$) were generated in the C57BL/6 background and characterized in previous studies[11,25].

Cloning, expression and purification of recombinant proteins
Human IgG1 Fc-domain variants were generated by site-directed mutagenesis using specific primers as previously described[9], and recombinant IgG antibodies were expressed and purified using previously described protocols[11]. Purity was assessed by SDS–PAGE followed by SafeStain blue staining (ThermoFisher), as well as by size exclusion chromatography (SEC) using a Superdex 200 Increase 10/300GL column (GE Healthcare) on an Äkta Pure 25 HPLC system (data analysed using Unicorn v.6.3 software). All antibody preparations were more than 94% pure and endotoxin levels were less than 0.05 EU mg^{-1}, as measured by the limulus amebocyte lysate assay.

The two plasmid-based HIV-NanoLuc-SARS-CoV-2 pseudovirus system[35] was provided by P. Bieniasz (Rockefeller University). The S gene was modified by site-directed mutagenesis to introduce the amino acid changes present in the MA10 or the B.1.351 strains[7]. SARS-CoV-2 wild-type, MA10 and B.1.351 pseudovirus particles were generated by transfection of the two-plasmid-based system to 293T cells using X-tremeGENE HP DNA transfection reagent (Sigma).

Golden Syrian hamster FcγR cDNA sequences were identified based on the current *M. auratus* genome assembly (MesAur1.0) and recent transcriptomic data[36]. To validate sequences, hamster FcγR sequences were amplified and sequenced (Genewiz) from Syrian hamster spleen cDNA (Zyagen) using the following primers: hamster FcγRI (5′-GGCGGACAAGTGGTAAATGTCAC-3′, 5′-CGGACACATCATTGCTTCAGACTTACTAAG-3′), hamster FcγRII (5′-CTGCTGGGACACATGATCTCC-3′, 5′-TTAAATGTGGTTCTGGTAATCATGCTCTG-3′), hamster FcγRIII (5′-GAGTCTGGAGACACAGATGTTTCAG-3′, 5′-CGACGTCATTTGTCCCGAGG-3′), hamster FcγRIV (5′-AATGGGTGAGGGTGCTTGAG-3′, 5′-GAGGGAATGTTGGGGACAGG-3′). To identify the ectodomain, transmembrane and cytoplasmic domains, Syrian hamster FcγR protein sequences were then aligned against annotated mouse FcγR protein sequences (Uniprot). Soluble Syrian hamster FcγR ectodomains were generated by transient transfection as described above for monoclonal antibodies. Syrian hamster FcγR expression plasmids were generated encoding a secretion signal peptide, the predicted Syrian hamster FcγR ectodomain, and a C-terminal Strep or His tag. Following transfection of Expi293 cells, recombinant FcγRs were purified from cell-free supernatants by affinity purification using Strep-Tactin Superflow Plus resin (Qiagen) or Ni-NTA Agarose (Qiagen), per manufacturer's instructions. Purified proteins were dialysed into PBS and assessed for purity by SDS–PAGE followed by SafeStain blue staining. Monomeric FcγR ectodomains were fractionated from aggregates by SEC on an Äkta Pure system using a Superdex 200 Increase 10/300 GL column (GE Healthcare).

Surface plasmon resonance
All experiments were performed with a Biacore T200 SPR system (GE Healthcare) at 25 °C in HBS-EP$^+$ buffer (10 mM HEPES, pH 7.4, 150 mM NaCl, 3.4 mM EDTA, 0.005% (v/v) surfactant P20). IgG antibodies were immobilized on Series S Protein G sensor chip (GE Healthcare) at a density of 2,000 response units (RU). Serial dilutions of recombinant soluble hamster FcγR ectodomains were injected to the flow cells at 20 μl min^{-1}, with the concentration ranging from 1,000 to 15.625 nM (successive 1:2 dilutions). Association time was 60 s followed by a 900-s dissociation step. At the end of each cycle, sensor surface was regenerated with a glycine HCl buffer (10 mM, pH 2.0; 50 μl min^{-1}, 30 s). Background binding to blank immobilized flow cells was subtracted, and affinity constants were calculated using BIAcore T200 evaluation software v.2.0 (GE Healthcare) using the 1:1 Langmuir binding model.

Neutralization assay
Neutralization activity of IgG1 Fc-domain variants was measured as previously described[35]. In brief, HT1080-ACE2 cells were seeded in 96 U-well black plates 24 h prior to infection with SARS-CoV-2 wild-type, MA10 or B.1.351 pseudoviruses. Pseudovirus particles were pre-incubated with monoclonal antibodies (fourfold serially diluted starting at 10 μg ml^{-1}) for 1 h at 37 °C and then added to a monolayer of HT1080$_{ACE2}$ cells. Following a 48-h incubation at 37 °C, cells were carefully washed with PBS and lysed with Luciferase Cell Culture Lysis reagent (Promega)

for 15 min. Nano luciferase activity was detected by adding Nano-Glo Luciferase Assay System (Promega) and measured by SpectraMax Plus spectrophotometer (Molecular Devices), using 0.5 s integration time. Data were collected and analysed using SoftMax Pro v.7.0.2 software (Molecular Devices). Relative luciferase units were normalized to those derived from cells infected with the relevant SARS-CoV-2 pseudoviruses in the absence of monoclonal antibodies.

Anti-SARS-CoV-2 RBD ELISA

Recombinant SARS-CoV-2 RBD was immobilized ($1 \mu g \text{ ml}^{-1}$) into high-binding 96-well microtitre plates (Nunc) and after overnight incubation at 4 °C, plates were blocked with PBS plus 2% (w/v) BSA for 2 h. After blocking, plates were incubated for 1 h with serially diluted IgG antibodies or serum samples (1:3 consecutive dilutions in PBS starting at 100 ng ml⁻¹), followed by horseradish peroxidase-conjugated goat anti-human IgG (1 h; 1:5,000; Jackson Immunoresearch). Plates were developed using the TMB two-component peroxidase substrate kit (KPL) and reactions were stopped with the addition of 1 M phosphoric acid. Absorbance at 450 nm was immediately recorded using a SpectraMax Plus spectrophotometer (Molecular Devices) and background absorbance from negative control samples was subtracted. Data were collected and analysed using SoftMax Pro v.7.0.2 software (Molecular Devices).

C1q-binding assay

Human and mouse C1q binding to IgG1 Fc variants was assessed following previously described protocols[37]. In brief, antibodies were serially diluted ($100–0.046 \mu g \text{ ml}^{-1}$) in PBS and coated overnight (4 °C) onto high-binding 96-well microtiter plates. After washing with PBS + 0.05% Tween-20, plates were blocked with 2% BSA. Normal mouse or human serum (3%) was added and incubated for 60 min with gentle shaking. For the detection of C1q binding, monoclonal mouse anti-C1q antibody (JL-1, Abcam) was added at 0.5 μg ml⁻¹, horseradish peroxidase-conjugated goat anti-mouse IgG was used at a dilution of 1:5,000, and plates were developed and analysed as described above.

Quantification of serum IgG levels

Blood was collected into microvette serum gel tubes (Sarstedt) and serum was fractionated by centrifugation ($10,000g$, 5 min). IgG levels were determined by enzyme-linked immunosorbency assay (ELISA) following previously described protocols[11].

In vivo SARS-CoV-2 infection models

All animal infection experiments were performed at the Comparative Bioscience Center of the Rockefeller University in animal biosafety level 3 (ABSL-3) containment in compliance with institutional and federal guidelines. Hamsters (6- to 8-week-old males) were anaesthetized with isoflurane (3%) in a VetFlo high-flow vaporizer followed by an intraperitoneal injection of a ketamine (150 mg kg⁻¹) and xylazine (10 mg kg⁻¹) mixture. Hamsters were challenged intranasally with 10⁵ pfu SARS-CoV-2 (NYC isolate, 100 μl viral inoculum). Mice (males or females; 6–7 or 16–22 weeks old) were anaesthetized with a ketamine (75 mg kg⁻¹) and xylazine (15 mg kg⁻¹) mixture (administered intraperitoneally) before challenge with SARS-CoV-2 (MA10 strain, 10⁴ pfu in 30 μl, intranasally).

No statistical method was used to predetermine sample size. On the basis of preliminary studies that determined experimental variation in survival following infection and monoclonal antibody treatment, we performed power calculations and determined that at least $n = 6$ animals per group is sufficient to detect differences among experimental groups (powered at 80% for 5% significance level; survival assessed by log-rank (Mantel–Cox) test).

After infection, animals were monitored daily and humanely euthanized by CO_2 asphyxiation at endpoints authorized by the Rockefeller University Institutional Animal Care and Use Committee, including any of the following: marked lethargy or inactivity, severe respiratory distress or laboured breathing, inability to ambulate or weight loss of greater than 20% of baseline. Animals were randomized on the basis of age, sex and weight. Before treatment, we ensured that the mean weight, sex and age were comparable among the various treatment groups. The treatment groups were not blinded to the personnel involved in monitoring animal survival and weight upon challenge. For antibody-mediated prophylaxis, antibodies were administered intravenously one day before virus challenge, whereas for antibody-mediated therapy, antibodies were administered one day after infection. Antibody dose was calculated in mg kg⁻¹ body weight.

Histological analysis

Lungs from euthanized mice were instilled with 10% neutral buffered formalin and fixed overnight by submersion in 10% formalin. Fixed tissues were embedded in paraffin, sectioned at 4-μm thickness, and stained with haematoxylin and eosin. Sections of lung were microscopically evaluated by a board-certified veterinary anatomic pathologist and representative images were captured with an Olympus BX45 light microscope using an SC30 camera with the cellSens Dimension software.

Determination of lung viral titres

Hamsters were euthanized at the indicated timepoints following infection and lung weights were recorded. Lungs were lysed in Trizol (ThermoFisher) and dissociated in gentle MACS M tubes using the gentleMACS Octo Dissociator (Miltenyi Biotec). Samples were transferred into Phasemaker tubes (ThermoFisher) and chloroform was added (200 μl chloroform per ml TRIzol). After vigorous shaking, tubes were rested for 5 min and then centrifuged for 15 min at $12,000g$ at 4 °C. The aqueous phase containing the RNA was transferred into a new tube and RNA extraction was performed by using RNeasy mini kit (Qiagen). SARS-CoV-2 lung titres were determined by quantitative PCR with reverse transcription assay using TaqMan Fast Virus 1-Step Master Mix, specifically designed primers and a TaqMan probe that bind a conserved region in the nucleocapsid gene of SARS-CoV-2 (2019-nCoV_N1-F :5′-GACCCCAAAATCAGCGAAAT-3′; 2019-nCoV_N1-R: 5-TCTGGTTACTGCCAGTTGAATCTG-3′; 2019-nCoV_N1-P: 5′-FAM-ACCCCGCATTACGTTTGGTGGACC-BHQ1-BHQ1-3′). Quantitative PCR was performed using an Applied Biosystems QuantStudio 6 Flex cycler using the following parameters: 50 °C for 5 min, 95 °C for 20 s followed by 40 cycles of 95 °C for 3 s, and 30 s at 60 °C. Signal from unknown samples was compared to a known standard curve (obtained through BEI Resources, NIAID, NR-52358) and viral titres were expressed as RNA copies per mg tissue.

Flow Cytometry

After lysis of red blood cells (RBC lysis buffer; Biolegend), cells were resuspended in PBS containing 0.5% (w/v) BSA and 5 mM EDTA and labelled with the following fluorescently labelled antibodies (all used at 1:200 dilution unless otherwise stated): anti-human FcγRIIa (clone IV.3)-FITC, anti-human FcγRIIb (clone 2B6)-Dylight650 (used at 5 μg ml⁻¹), anti-B220-AlexaFluor700, anti-Gr1-BrilliantViolet421, anti-CD8β-BrilliantViolet510, anti-human FcγRI (clone 10.1)-BrilliantViolet605, anti-CD3-BrilliantViolet650 (used at 1:100 dilution), anti-CD11b-BrilliantViolet711, anti-CD4-BrilliantViolet785, anti-human FcγRIIIa/b (clone 3G8)-PE, and anti-NK1.1–PE–Cy7. Relevant isotype control antibodies were used and included: mouse IgG1 isotype control-Dylight650 (used at 5 μg ml⁻¹), mouse IgG2b kappa isotype control–FITC, mouse IgG1 kappa isotype control–PE, mouse IgG1 kappa isotype control–BrilliantViolet605. Samples that were stained with isotype control antibodies were also blocked with unlabeled anti-FcγR antibodies as follow: anti-human FcγRI (clone 10.1), anti-human FcγRIIa (clone IV.3), anti-human FcγRIIb (clone 2B6), and anti-human FcγRIIIa/b (clone 3G8) (used at 10 μg ml⁻¹ and incubated for 5 min before staining with fluorescently labelled

antibodies). Samples were analysed on an Attune NxT flow cytometer (ThermoFisher) using Attune NxT software v3.1.2 and data were analysed using FlowJo (v10.7) software.

Statistical analysis

Raw data for all main and extended data figures are included in the manuscript as source files. Results from multiple experiments are presented as mean ± s.e.m. One- or two-way ANOVA was used to test for differences in the mean values of quantitative variables, and where statistically significant effects were found, post hoc analysis using Bonferroni (adjusted for multiple comparisons) test was performed. Statistical differences between survival rates were analysed by comparing Kaplan–Meier curves using the log-rank (Mantel–Cox) test. Data were collected and analysed with Microsoft Excel and GraphPad Prism v.9.1 software (GraphPad) and $P < 0.05$ was considered to be statistically significant.

Reporting summary

Further information on research design is available in the Nature Research Reporting Summary linked to this paper.

Data availability

Raw data for all main and extended data figures are included in the manuscript as source files. Source data are provided with this paper.

34. Blight, K. J., McKeating, J. A. & Rice, C. M. Highly permissive cell lines for subgenomic and genomic hepatitis C virus RNA replication. *J. Virol.* **76**, 13001–13014 (2002).
35. Schmidt, F. et al. Measuring SARS-CoV-2 neutralizing antibody activity using pseudotyped and chimeric viruses. *J. Exp. Med.* **217**, e20201181 (2020).
36. McCann, K. E., Sinkiewicz, D. M., Norvelle, A. & Huhman, K. L. De novo assembly, annotation, and characterization of the whole brain transcriptome of male and female Syrian hamsters. *Sci. Rep.* **7**, 40472 (2017).
37. Pietzsch, J. et al. A mouse model for HIV-1 entry. *Proc. Natl Acad. Sci. USA* **109**, 15859–15864 (2012).

a

Syrian hamster FcγRI

MWLLTTLLLWVPVGGQVVNVTKAVVTLQPPWVSIFLKENVTLWCEGLHPP
GDRTTRWFINSTALQISTPSYSITEATLKDSGEYRCQTGLSMPSDPVQLE
IHRDWLLLQASDRVLTEGKPLTLRCHGWQSKMVYNVVFYRDGKYFHSSQD
SEVTILQTNLTHSGVYHCAGIGRHYRYTSAGMSVTVKELFATPVLTASL
SSPFPEGSPVTLSCVTKLPPQSPGLQLYFSFYVGSETLEDRKTSAEYHIP
SAKREDSGLYWCEAATEDGSVRKRSPELELRTPGPQSSGPVWFHILFYLS
MGIIFLVDTVLCAKIRKKLQRKKNYNLEVLLVSDQGKKETSS

Syrian hamster FcγRIIb

MLLWTAVLNLAAGTHDLPKAMVKLEPPWIQVLKEDRVTLKCEGTHSPGND
STQWLHNGNSLWSQVQPSYTFKASDNDSGEYQCRMGQTSLSDPVQLGVIS
DWLLLQTPQLVFEEGETIVLRCHSWRNKFMSKVTFYHNGKSIRYNHFISN
VSIAKANHSHSGDYHCTARLGQAQHSSRPVTITVQEPRSSGSLPILTIVA
AVTGIAVAAIVIILVSLIYLRKQAPALPGNPDHREKGDTLPKEQGEYSV
PSGDSVPVSPGPPCCGQEPASNSSYNSPDLEEAAKTEVENTITYSLLKHPE
APDEDAEHDYQNHI

Syrian hamster FcγRIII

MFQNVHSGSQWLLQPLTILLLFALADRQTADLPKAVVKLEPPWIQVLKED
RVTLKCEGTHSPGNDSTQWLHNGNSLWSQVQPSYTFKASDNDSGEYQCRM
GQTSLSDPVQLGVISDWLLLQTPQLVFEEGETIVLRCHSWRNKFMSKVTF
YHNGKSIRYNHFISNISIAKANHSHSGDYHCTARLGQAQHSSRPVTITVQ
GPSTTPFTSLLWYHAAFCLVMCLLFAVDTGLYFYVQRNLQAPVEKWRKTL
SVRKCQAPRDK

Syrian hamster FcγRIV

MWQLLLPTALLLIVSSGIRAGLRKAVVTLHPEWVRVLEEDSVTLRCQGTY
APGDNSTKWFHNGSLTSQQDTNYVIGSAKVKDSGEYKCQTALSTASDPVN
LEVHIGWLLLQTTQRPVFQEGDPIRLKCHSWRNKTVYKVTYLQNGKGKKY
FHKNSELYIPNATQNHSGSYFCRGLIGQNNKSSETLRIIVGVLPPDLTPP
SNNFPPWHQITFCLLIGLLFTIDTVLYFSVQRGLRRSTADYEEPDLHWSK
EPEDKTISEEKQSFRSSRVNSETPSGGSRPPEK

b

Human IgG1 Fc Variant	FcγRI		FcγRIIb		FcγRIII		FcγRIV	
	KD (M)	Fold	KD (M)	Fold	KD (M)	Fold	KD (M)	Fold
Wild Type	7.37×10^{-7}	1.00	$>1.0\times10^{-6}$	1.00	$>1.0\times10^{-6}$	1.00	1.02×10^{-7}	1.0
V11	$>1.0\times10^{-6}$	<0.74	3.45×10^{-7}	>2.9	2.60×10^{-7}	>3.9	$>1.0\times10^{-6}$	<0.1
GAALIE	$>1.0\times10^{-6}$	<0.74	3.28×10^{-7}	>3.0	2.33×10^{-7}	>4.3	9.52×10^{-9}	10.7
GRLR	n.d.b.		n.d.b.		n.d.b.		n.d.b.	

c

Mouse IgG	FcγRI		FcγRIIb		FcγRIII		FcγRIV	
	KD (M)	Fold	KD (M)	Fold	KD (M)	Fold	KD (M)	Fold
IgG1	$>1.0\times10^{-6}$	1.0	1.43×10^{-7}	1.0	7.81×10^{-8}	1.0	$>1.0\times10^{-6}$	1.0
IgG2a	3.38×10^{-7}	>3.0	1.14×10^{-6}	0.12	5.72×10^{-7}	0.13	1.47×10^{-8}	>68
IgG1-D265A	n.d.b.		n.d.b.		n.d.b.		n.d.b.	

d

Hamster IgG	FcγRI		FcγRIIb		FcγRIII		FcγRIV	
	KD (M)	Fold	KD (M)	Fold	KD (M)	Fold	KD (M)	Fold
IgG1	$> 1.0\times10^{-6}$	1.0	5.62×10^{-8}	1.0	3.55×10^{-8}	1.0	$> 1.0\times10^{-6}$	1.0
IgG2	4.96×10^{-7}	>2	1.03×10^{-6}	0.05	7.02×10^{-7}	0.04	1.71×10^{-8}	> 58
IgG1-D265A	n.d.b.		n.d.b.		n.d.b.		n.d.b.	

e

Extended Data Fig. 1 | Cloning and characterization of the IgG binding activity of hamster FcγRs. a, Syrian hamster FcγRs were cloned, and their sequences were determined. The FcR ectodomains are underlined. **b-e**, The affinity of human IgG1 and Fc variants (**b**, **e**, SPR sensorgrams), as well as of mouse (**c**) and hamster (**d**) IgG subclass variants for the various classes of hamster FcγRs was determined by surface plasmon resonance (SPR), using soluble hamster FcγR ectodomains. n.d.b., no detectable binding.

Extended Data Fig. 2 | Comparison of the FcγR expression levels in the various effector leukocyte populations between young and older FcγR humanized mice. FcγR expression was assessed by flow cytometry in peripheral blood leukocyte populations from young (6-7 weeks old; orange) and older (17 weeks old; blue) FcγR humanized mice. **a**, Gating strategy to identify the various leukocyte populations, **b**, Representative histogram overlay plots of FcγR expression in young and older FcγR humanized mice. Corresponding isotype controls are indicated in lighter shade. **c**, Quantitation of FcγR expression (MFI, median fluorescence intensity subtracted from the respective isotype control) in various leukocyte populations. Results are from 4 or 5 mice per group for young and older mice, respectively.

Article

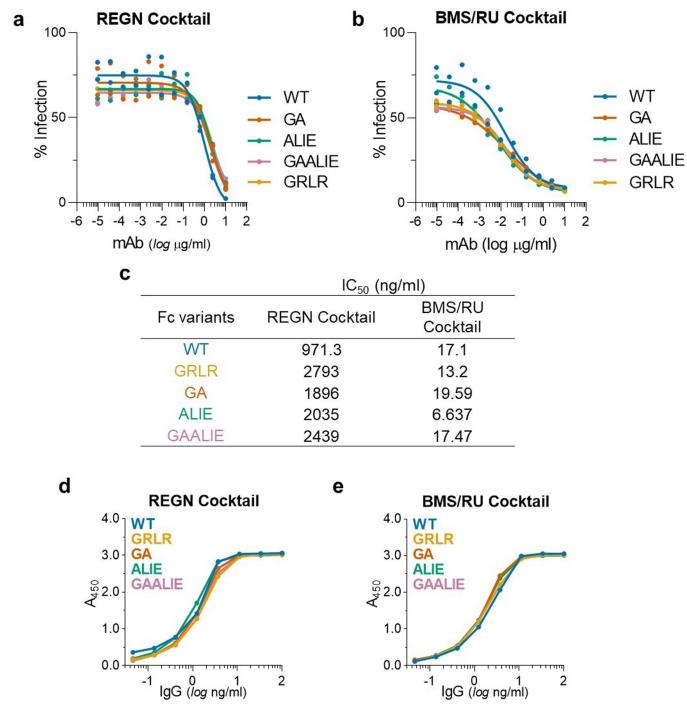**Extended Data Fig. 3 | Histopathological analysis of lung tissue from SARS-CoV-2-infected FcγR humanized mice.** Lungs from SARS-CoV-2-infected (MA10 strain, 10^4 pfu, i.n.) FcγR humanized mice (16-22 weeks old) were collected on day 4 post-infection and evaluated histologically to assess the pathological changes associated with SARS-CoV-2 infection. **a**, Uninfected mice were characterized by clear alveolar spaces and absence of inflammatory cell infiltrates (low magnification (left panel, 200x); high magnification (center and right panels, 400x). **b**, In contrast, SARS-CoV-2 infection was associated with perivascular and peribronchial mononuclear leukocyte infiltration (200x left; 400x center panel), as well as the presence of macrophages and neutrophils in alveoli and necrotic cellular debris in alveolar spaces (600x, right panel). **c**, In addition, SARS-CoV-2-infected mice exhibited perivenular mixed neutrophilic, histiocytic, and lymphocytic inflammation, reactive endothelium and extravasation of leukocytes (left panel, 400x), as well as foci of interstitial neutrophilic and macrophage inflammation with hemorrhage and single cell necrosis (center and right panels, 400x). Images are representative of one uninfected and six infected mice.

a

| REGN 10933 | REGN 10987 | REGN Cocktail (10933+10987) | C135 | C144 | BMS/RU Cocktail (C135+C144) |

y-axis: % Infection (100, 50) *x-axis:* mAb (log μg/ml) −6 −5 −4 −3 −2 −1 0 1 2

Legend: SARS-CoV-2$_{WT}$; SARS-CoV-2$_{MA10}$; SARS-CoV-2$_{B.1.351}$

b

mAb	IC$_{50}$ (ng/ml)		
	SARS-CoV-2$_{WT}$	SARS-CoV-2$_{MA10}$	SARS-CoV-2$_{B.1.351}$
REGN 10933	2.406	609.6	491.8
REGN 10987	7.515	>10000	2.852
REGN cocktail	2.713	1302	1.995
BMS/RU C135	2.287	13.78	2.195
BMS/RU C144	2.089	>10000	>10000
BMS/RU cocktail	2.194	22.12	3.291

c

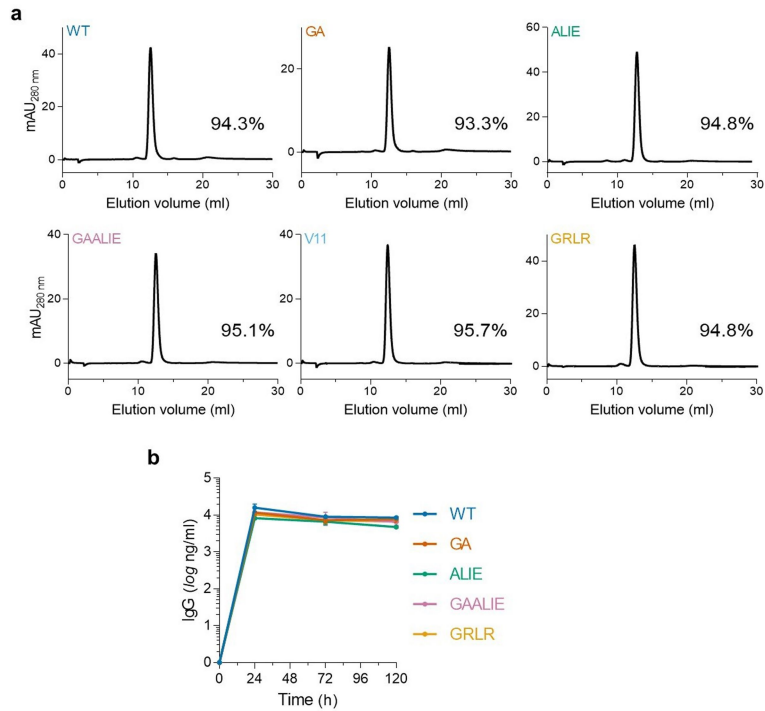| mAb	Fold change over WT		
	SARS-CoV-2$_{WT}$	SARS-CoV-2$_{MA10}$	SARS-CoV-2$_{B.1.351}$
REGN 10933	1	253.4	204.4
REGN 10987	1	1330.7	0.4
REGN cocktail	1	479.9	0.7
BMS/RU C135	1	6	0.95
BMS/RU C144	1	4786.9	4786.9
BMS/RU cocktail	1	10	1.5

d

Extended Data Fig. 4 | In vitro neutralization activity of anti-SARS-CoV-2 mAbs against SARS-CoV-2 strains. Neutralization activity of REGN and BMS/RU mAbs (individual mAbs or as a cocktail) against SARS-CoV-2 pseudotyped reporter viruses was measured by *in vitro* neutralization assay. (**a**) *In vitro* neutralization curves and (**b**) IC$_{50}$ values of REGN (upper panel) and BMS/RU (lower panel) against SARS-CoV-2 WT, MA10, or B.1.351. (**c**) Fold change of SARS-CoV-2$_{MA10}$ and SARS-CoV-2$_{B.1.351}$ IC$_{50}$ was calculated over WT. n = 1 experiment performed in duplicates. (**d**) Cryo-EM structures of REGN10933 and REGN10987 complexed with SARS-CoV-2 (PDB: 6XDG) or C135 (PDB: 7K8Z) and C144 (PDB: 7K90) complexed with the SARS-CoV-2 spike trimer. Residues within the SARS-CoV-2$_{WT}$ RBD that are mutated in the SARS-CoV-2$_{MA10}$ strain (Q493K, Q498Y, P499T) are indicated in magenta.
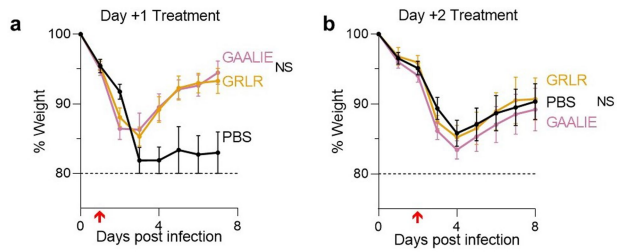
Article

Extended Data Fig. 5 | *In vitro* neutralization activity and antigenic specificity of Fc variants of anti-SARS-CoV-2 mAbs. To confirm that changes in the Fc domain have no effect on the neutralization activity and Fab-mediated functions of anti-SARS-CoV-2 mAb, Fc domain variants were characterized in (**a-c**) *in vitro* neutralization assays using SARS-CoV-2$_{MA10}$ pseudotyped reporter viruses and (**d, e**) in ELISA assays using SARS-CoV-2 RBD. n = 1 experiment performed in duplicates. (**a, d**) REGN and (**b, e**) BMS/RU mAb cocktails were expressed as Fc variants and their *in vitro* neutralization activity (**a, b, c**, IC$_{50}$ values) and (**d, e**) antigenic specificity was compared among Fc variants.

a

b

Extended Data Fig. 6 | *In vitro* and *in vivo* stability of Fc variants of anti-SARS-CoV-2 mAbs. (a) Size-exclusion chromatography (SEC) analysis of Fc variants to determine aggregate formation among Fc domain variants. The SEC elution profiles and abundance (percentage) of monomeric IgG is indicated for the different Fc variants. (**b**) Fc variants of the REGN mAb cocktai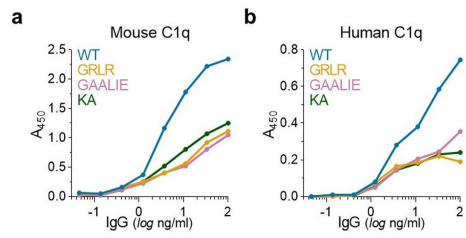l were administered (i.v.; 50 μg) to FcγR humanized mice and antibody serum levels were determined by ELISA at various time points after antibody administration. n = total of 3 mice per group from two independent experiments. Data are mean ± s.e.m.

Article

Extended Data Fig. 7 | High-dose treatment of SARS-CoV-2-infected FcγR humanized mice with anti-SARS-CoV-2 mAbs Fc variants enhanced for activating FcγR binding is not associated with enhanced disease.
(**a**) Following the experimental strategy in Fig. 3b, SARS-CoV-2-infected (MA10, 10^4 pfu, i.n.) FcγR humanized mice (n = 3 for PBS and n = 5 for mAb-treated groups) were treated (i.v.) with 40 mg/kg REGN mAb cocktail expressed as Fc variants with diminished (GRLR) or enhanced activating FcγR binding (GAALIE). (**b**) SARS-CoV-2-infected mice were treated with 10 mg/kg BMS/RU mAb cocktail expressed as Fc variants GRLR or GAALIE on day 2 post infection. n= total of 10 mice per group for PBS, n = 9 for GAALIE, and n = 6 for GRLR from two independent experiments Weight loss (mean ± s.e.m.) was compared between GRLR and GAALIE-treated groups by two-way ANOVA (Bonferroni post hoc analysis adjusted for multiple comparisons). NS, not significant. Red arrow indicates time point of mAb treatment post-infection.

Extended Data Fig. 8 | Mouse and human C1q binding of Fc domain variants of IgG1. The capacity of IgG1 Fc domain variants to interact with mouse (**a**) and human (**b**) C1q was assessed by ELISA (n = 1 experiment performed in duplicates). The KA (K322A) variant, which has previously described as a complement-deficient mutant[28], was included as control.

nature research

Corresponding author(s):	Jeffrey Ravetch and Stylianos Bournazos
Last updated by author(s):	Sep 6, 2021

Reporting Summary

Nature Research wishes to improve the reproducibility of the work that we publish. This form provides structure for consistency and transparency in reporting. For further information on Nature Research policies, see our Editorial Policies and the Editorial Policy Checklist.

Statistics

For all statistical analyses, confirm that the following items are present in the figure legend, table legend, main text, or Methods section.

n/a	Confirmed	
☐	☒	The exact sample size (*n*) for each experimental group/condition, given as a discrete number and unit of measurement
☐	☒	A statement on whether measurements were taken from distinct samples or whether the same sample was measured repeatedly
☐	☒	The statistical test(s) used AND whether they are one- or two-sided *Only common tests should be described solely by name; describe more complex techniques in the Methods section.*
☐	☒	A description of all covariates tested
☐	☒	A description of any assumptions or corrections, such as tests of normality and adjustment for multiple comparisons
☐	☒	A full description of the statistical parameters including central tendency (e.g. means) or other basic estimates (e.g. regression coefficient) AND variation (e.g. standard deviation) or associated estimates of uncertainty (e.g. confidence intervals)
☐	☒	For null hypothesis testing, the test statistic (e.g. *F*, *t*, *r*) with confidence intervals, effect sizes, degrees of freedom and *P* value noted *Give P values as exact values whenever suitable.*
☒	☐	For Bayesian analysis, information on the choice of priors and Markov chain Monte Carlo settings
☒	☐	For hierarchical and complex designs, identification of the appropriate level for tests and full reporting of outcomes
☒	☐	Estimates of effect sizes (e.g. Cohen's *d*, Pearson's *r*), indicating how they were calculated

Our web collection on statistics for biologists contains articles on many of the points above.

Software and code

Policy information about availability of computer code

Data collection	GE Unicorn v6.3, SoftMaxPro v7.0.2, Biacore T200 control software v2.0, Attune NxT flow cytometry software v3.1.2, Microsoft Excel, Applied Biosystems QuantStudio 6 Flex Real-Time PCR, software v1.3, Olympus BX45 light microscope with an SC30 camera, Illumina MiSeq
Data analysis	GE Unicorn v6.3, SoftMaxPro v7.0.2, Biacore T200 evaluation software v2.0, QuantStudio Real-Time PCR Software v1.3, Graphpad Prism v9, Microsoft Excel v2008, SeqBuilder Pro v16 and v17, SeqMan Pro v16 and v17, Olympus cellSens Dimension software, FlowJo v10.7.

For manuscripts utilizing custom algorithms or software that are central to the research but not yet described in published literature, software must be made available to editors and reviewers. We strongly encourage code deposition in a community repository (e.g. GitHub). See the Nature Research guidelines for submitting code & software for further information.

Data

Policy information about availability of data

All manuscripts must include a data availability statement. This statement should provide the following information, where applicable:
- Accession codes, unique identifiers, or web links for publicly available datasets
- A list of figures that have associated raw data
- A description of any restrictions on data availability

Raw data for all main and extended data figures are included in the manuscript as source files.

Field-specific reporting

Please select the one below that is the best fit for your research. If you are not sure, read the appropriate sections before making your selection.

☒ Life sciences   ☐ Behavioural & social sciences   ☐ Ecological, evolutionary & environmental sciences

For a reference copy of the document with all sections, see nature.com/documents/nr-reporting-summary-flat.pdf

Life sciences study design

All studies must disclose on these points even when the disclosure is negative.

Sample size	No statistical method was used to predetermine sample size. For in vivo experiments, based on preliminary studies that determined experimental variation in survival following infection and mAb treatment, we have performed power calculations and determined that at least n=6 mice/group is sufficient to detect differences among experimental groups (powered at 80% for 5% significance level; survival assessed by log-rank (Mantel-Cox) test). For in vitro experiments, assays were performed using the indicated sample sizes to ensure reproducibility.
Data exclusions	No data were excluded.
Replication	The reported findings have been confirmed in large groups of mice/experimental group in multiple (>2) experiments. The enhanced protective activity of the Fc engineered variants was confirmed in multiple experiments using a variety of mAbs that target different epitopes on SARS-CoV-2 Spike protein. Also, two different challenge virus strains have been used (NY isolate and MA10) in two different animal models (hamsters and mice, respectively) to minimize strain-specific effects.
Randomization	Mice were randomized based on age, gender, and weight. Prior to treatment, we ensured that the mean weight and age were comparable among the various treatment groups. No randomization was used for the in vitro experiments, as it is not applicable to the study design. In vitro experiments did not involve experimental groups with different treatment conditions.
Blinding	Blinding is not relevant for this study, as this is an observational (not case-control) study.

Reporting for specific materials, systems and methods

We require information from authors about some types of materials, experimental systems and methods used in many studies. Here, indicate whether each material, system or method listed is relevant to your study. If you are not sure if a list item applies to your research, read the appropriate section before selecting a response.

Materials & experimental systems

n/a	Involved in the study
☐	☒ Antibodies
☐	☒ Eukaryotic cell lines
☒	☐ Palaeontology and archaeology
☐	☒ Animals and other organisms
☒	☐ Human research participants
☒	☐ Clinical data
☒	☐ Dual use research of concern

Methods

n/a	Involved in the study
☒	☐ ChIP-seq
☐	☒ Flow cytometry
☒	☐ MRI-based neuroimaging

Antibodies

Antibodies used	The clones of the recombinant anti-SARS-CoV-2 antibodies are reported in the manuscript and their characteristics are also described in previously published studies (relevant citations included in the manuscript).
	For ELISA assays, the following antibodies were used: HRP-conjugated goat F(ab')2 anti-human IgG (H+L)(Jackson Immunoresearch, 109-036-088, Lot: 147433, 1:5000); Biotin-conjugated goat F(ab')2 anti-human IgG (F(ab')2-specific)(Jackson Immunoresearch, 109-066-088, Lot: 139987 5 μg/ml); Mouse anti-C1q antibody (Abcam, ab71940).
	The following antibodies were used for flow cytometry (unless otherwise noted, all antibodies were used at 1:200 dilution): anti-B220-AF700 (Biolegend, 103232, RA3-6B2, B272460) anti-Gr-1-BV421 (Biolegend, 108445, RB6-8C5, B292607) anti-CD8b-BV510 (Biolegend, 126631, YTS156.7.7, B303593) anti-CD3-BV650 (Biolegend, 100229, 17A2, B282105, used at 1:100 dilution) anti-CD11b-BV711 (Biolegend, 101242, M1/70, B315411) anti-CD4-BV785 (Biolegend, 100453, GK1.5, B284013) anti-NK1.1-PE/Cy7 (Invitrogen, 25-5941-82, PK136, 1981963) anti-human FcγRI-BV605 (Biolegend, 305034, 10.1, B293272) anti-human FcγRIIa-FITC (Stemcell technologies, 60012FI, IV.3)

anti-human FcγRIIb-Dylight650; (clone 2B6, produced in house and conjugated with Dylight650 kit)
anti-human FcγRIIIa/b-PE (Biolegend, 980102, 3G8, B301142)
Mouse IgG1 isotype control-Dylight650 (ThermoFisher, MA1-191-D650, MOPC-21)
Mouse IgG2b kappa isotype control - FITC (ThermoFisher, 11-4732-42, eBMG2b)
Mouse IgG1 kappa isotype control-PE (Biolegend, 400112, MOPC-21, B291605)
Mouse IgG1 kappa isotype control-BV605 (Biolegend, 400162, MOPC-21, B329915)
anti-human FcγRI (Biolegend, 305048, 10.1, B303217)
anti-human FcγRIIa (Stemcell technologies, 60012, IV.3)
anti-human FcγRIIb (clone 2B6, produced in house)
anti-human FcγRIIIa/b (Biolegend, 302049, 3G8)

Validation

For recombinant anti-SARS-CoV-2 mAbs, their antigenic specificity and neutralization activity were assessed in in vitro assays (data presented in the manuscript Extended Data Figure 5) to ensure that changes in the Fc domain have no impact on their Fab-mediated activities. Purity of recombinant proteins was assessed by SDS-PAGE followed by SafeStain blue staining (ThermoFisher) and SEC. All antibody preparations were >94% pure and endotoxin levels were <0.05 EU/mg, as determined by the Limulus Amebocyte Lysate (LAL) assay.

For commercially available antibodies, validation has been performed by the manufacturer and corresponding certificates of analysis are available at the manufacturer's website. Specificity is tested in 1-3 target cell types with either single- or multi-color analysis (including positive and negative cell types). Once specificity is confirmed, each new lot is validated to ensure that it performs with similar intensity to the in-date reference lot. Brightness (MFI) is evaluated from both positive and negative populations. Each lot product is validated by QC testing with a series of titration dilutions.

The specificity of antibodies used for ELISA were validated by the manufacturer by immunoelectrophoresis and/or ELISA. No reactivity was detected against non-immunoglobulin serum proteins. Antibodies are also tested by the manufacturer by ELISA and/or solid-phase adsorbed to ensure minimal cross-reaction with immunoglobulins from other species.

Eukaryotic cell lines

Policy information about cell lines

Cell line source(s)

VeroE6, Caco-2, 293T - ATCC
Expi293F - ThermoFisher
Huh7.5 - Charles Rice laboratory, Rockefeller University
HT1080-ACE2 - Paul Bieniasz laboratory, Rockefeller University

Authentication

Cell lines were not authenticated after purchase

Mycoplasma contamination

All cell lines have been tested by the manufacturer and were tested negative for mycoplasma contamination. Certificates of analysis are available in manufacturer's website. All cell lines were maintained for <10 passages to minimize mycoplasma contamination. Media and supplements (FBS) were also all mycoplasma-free (per certificate of analysis).

Commonly misidentified lines
(See ICLAC register)

No commonly misidentified cell lines were used in this study.

Animals and other organisms

Policy information about studies involving animals; ARRIVE guidelines recommended for reporting animal research

Laboratory animals

Syrian golden hamsters (strain code 049) were purchased from Charles River laboratories. Males, 6-8 wk old hamsters were used. FcγR knockout (mFcγRα–/–; Fcgr1–/–) and FcγR humanized mice (mFcγRα–/–, Fcgr1–/–, hFcγRI+, hFcγRIIaR131+, hFcγRIIb+, hFcγRIIIaF158+, and hFcγRIIIb+) were generated in the C57BL/6 background and characterized in previous studies. Males or females; 6-7 or 16-22 weeks old mice were used in this study.
Hamsters and mice were housed at a controlled ambient temperature (20-25oC) and humidity (30-70%) environment with 12-hour light/dark cycle.

Wild animals

No wild animals were used in this study.

Field-collected samples

No field-collected samples were used in this study.

Ethics oversight

All in vivo experiments were performed in compliance with federal laws and institutional guidelines and have been approved by the Rockefeller University Institutional Animal Care and Use Committee. In-vivo experiments in hamsters were also in compliance with USDA regulations.

Note that full information on the approval of the study protocol must also be provided in the manuscript.

Flow Cytometry

Plots

Confirm that:

☒ The axis labels state the marker and fluorochrome used (e.g. CD4-FITC).

☒ The axis scales are clearly visible. Include numbers along axes only for bottom left plot of group (a 'group' is an analysis of identical markers).

☒ All plots are contour plots with outliers or pseudocolor plots.

☒ A numerical value for number of cells or percentage (with statistics) is provided.

Methodology

Sample preparation	Mouse blood was collected from the retro-orbital venous plexus. Following RBC lysis (RBC lysis buffer; Biolegend), single cell suspensions were resuspended in PBS containing 0.5% (w/v) BSA and 5 mM EDTA. Cells were labeled with mixtures of fluorescently labeled antibodies incubated at 4C for 15 min and washed twice with PBS containing 0.5% (w/v) BSA and 5 mM EDTA prior to analysis.
Instrument	0A29009 Attune NxT Acoustic Focusing Cytometer (Lasers: BRV6Y)
Software	For data acquisition, Attune NxT flow cytometry software v3.1.2 was used. For data analysis, FlowJo v10.7 was used.
Cell population abundance	No sorting performed
Gating strategy	The gating strategy is presented in Extended Data Figure 2. Single cells were identified in FSC-A vs. FSC-H plots. For analysis of FcR expression on mouse blood cells, single cell leukocytes (identified based on FSC-A vs. FSC-H and SSC-A vs. FSC-A plots) are gated as B220 vs. CD3 to identify B220+ and CD3+ cells. CD3+ events are plotted as CD8 vs. CD4 to identify CD8 (CD8+/CD4-) and CD4 (CD4+/CD8-) T cells. B220-/CD3- cells are plotted as NK1.1 vs. CD11b to identify NK cells (gated as NK1.1+) and CD11b+ cells. CD11b+ were further plotted as SSC vs. Gr1. Neutrophils are identified as CD11b+/SSC+/Gr1+ cells. Gr1- monocytes are identified as CD11b+/SSC-/Gr1- cells. Gr1+ monocytes are identified as CD11b+/SSC-/Gr1+ cells.

☒ Tick this box to confirm that a figure exemplifying the gating strategy is provided in the Supplementary Information.